



Effect of initial nickel particle size on stability of nickel catalysts for aqueous phase reforming[☆]

Tomas van Haasterecht^a, Marten Swart^a, Krijn P. de Jong^a, Johannes Hendrik Bitter^{a,b,*}

^aInorganic Chemistry and Catalysis, Utrecht University, 3508 TB Utrecht, The Netherlands

^bBiobased Chemistry and Technology, Wageningen University, 6708 WG Wageningen, The Netherlands

ARTICLE INFO

Article history:

Received 26 October 2015

Revised 18 December 2015

Accepted 21 December 2015

Available online 13 January 2016

Keywords:

Aqueous phase reforming

Particle growth

Catalyst stability

Ostwald ripening

Leaching

Nickel catalysts

Particle size effect

Support effect

ABSTRACT

The deactivation behavior by crystallite growth of nickel nanoparticles on various supports (carbon nanofibers, zirconia, SiC, α -Al₂O₃ and γ -Al₂O₃) was investigated in the aqueous phase reforming of ethylene glycol. Supported Ni catalysts of ~10 wt% were prepared by impregnation of carbon nanofibers (CNF), ZrO₂, SiC, γ -Al₂O₃ and α -Al₂O₃. The extent of the Ni nanoparticle growth on various support materials follows the order CNF ~ ZrO₂ > SiC > γ -Al₂O₃ >> α -Al₂O₃ which sequence, however, was determined by the initial Ni particle size. Based on the observed nickel leaching and the specific growth characteristics; the particle size distribution and the effect of loading on the growth rate, Ostwald ripening is suggested to be the main mechanism contributing to nickel particle growth. Remarkably, initially smaller Ni particles (~12 nm) supported on α -Al₂O₃ were found to outgrow Ni particles with initially larger size (~20 nm). It is put forward that the higher susceptibility with respect to oxidation of the smaller Ni nanoparticles and differences in initial particle size distribution are responsible for this behavior.

© 2016 Science Press and Dalian Institute of Chemical Physics. All rights reserved.

1. Introduction

The use of biomass as a resource for the production of renewable fuels and especially chemicals is of increasing interest because of its potential role in the transition towards a more sustainable use of our natural resources. In order to efficiently process biomass (derived) resources into useful chemical and fuels the use of catalytic processes is invaluable. This requires the design of catalyst stable under the conditions typically employed for such process. For example the oxidation, hydrogenation, hydrogenolysis and reforming or biomass derived sugars all take place in the aqueous phase at elevated temperatures and pressures using supported metal catalysts. Platinum based catalysts are often employed in these processes but, because of the high cost and low abundance of Pt, alternatives are highly sought-after. Nickel has been proposed as alternative to Pt for the production of renewable hydrogen via the aqueous phase reforming of sugars and sugar like substrates (poly-

ols) [1–3]. Although it was found that Ni is less selective toward H₂ production due to methanation [1], this can be suppressed by alloying with e.g. Sn [4]. The stability of nickel is however still an issue for these catalysts and the loss of dispersion due to nickel particle growth is the main reason for the deactivation of carbon nanofiber (CNF) supported nickel catalyst in the aqueous phase [1].

Understanding the growth process of supported metal particles is of vital importance in order to develop strategies to improve catalyst stability. The growth of Ni [5] and other metal particles [6–8] has been investigated extensively in gas phase reactions [9]. Much less attention has been devoted to the growth of metal particles in the liquid or aqueous phase. Deactivation of Cu [3,10] and Ni [2,11] in the aqueous phase as a result of particle growth has been reported but studies on the growth kinetics of metal particles in the liquid phase have mainly focused on supported platinum catalyst [12–17] at low temperatures [15–17]. The growth of supported metal particles is also of interest in the design of stable fuel cell electrodes, especially low temperature PEM cells. Here significant work has been done focusing on the particle growth mechanism for the synthesis of stable electrodes, although again with a focus on Pt as the active phase. This often involves investigation of the growth characteristics of supported Pt nanoparticles in water or electrolyte solutions under induced accelerated aging with via a potential sweep. Morgan et al. reviewed the literature on mechanisms of surface area loss of platinum electrodes [18]. They

[☆] This research has been performed within the framework of the CatchBio program. The authors gratefully acknowledge the support of the Smart Mix Program of The Netherlands Ministry of Economic Affairs, Agriculture and Innovation and The Netherlands Ministry of Education, Culture and Science (Grant no. 053.70.011).

* Corresponding author at: Inorganic Chemistry and Catalysis, Utrecht University, 3508 TB Utrecht, The Netherlands. Tel: +31 317480303.

E-mail address: harry.bitter@wur.nl (J.H. Bitter).

concluded that platinum loss occurs due to platinum dissolution and platinum particle growth occurs due to Ostwald ripening (OR) but the role of particle migration and coalescence (PMC) is uncertain. Like in the gas phase the growth of metal particles in the liquid phase might proceed via two very different mechanisms, i.e. via Ostwald ripening (OR) or particle migration and coalescence (PMC) [19]. The driving force for the growth of (metal) particles via both mechanisms is the minimization of the total surface free energy of the system.

The growth of supported metal nanoparticles via migration and coalescence, also called sintering (sintering is used by some authors to exclusively denote particle growth via the particle migration and coalescence mechanism while others have used it as an umbrella term that encompassed both particle growth via Ostwald ripening and growth via particle migration and coalescence, Ostwald ripening is then referred to as chemical sintering while migration and coalescence is referred to as thermal sintering) or thermal sintering, involves the random motion of particles over the support resulting in collision with other mobile or immobile particles and their subsequent merger into a larger particle (coalescence). The migration of the particles does not necessarily occur as a concurrent movement of the entire particle, but probably results from an overall but random mass transfer of (ad)atoms from the particle to the support surface [19]. This mechanism generally occurs at high temperatures since a high mobility of the atoms is required for this mechanism. In other words this is a highly activated process and for gas phase reactions this generally occurs around temperatures of about half the melting point of the bulk metal (Tammann temperature), e.g. 590 °C for nickel. While the temperature in aqueous phase processes is substantially lower (e.g. 200 °C this study) this does not exclude thermal sintering as a particle growth mechanism a priori, since (liquid) water can affect the properties of metal nanoparticles and the mobility of the particles on the support differently than a gaseous environment.

The second mechanism, called Ostwald ripening or particle coarsening, is a mechanism of inter-particle migration by which molecules or atoms migrated from the smaller particles fixed on the support to the larger particles. The molecular or atomic species migrate either through a second phase (gas phase/solution, i.e. gaseous or ionic species) or via the support (adatoms). These different transport modes are denoted three dimensional (3D) and two dimensional (2D) Ostwald ripening respectively. The different mechanisms, PMC and 3D or 2D OR, are not mutually exclusive [20] and the dominating mechanism might even change during the growth process [19]. This makes the determination of the mode by which supported metal particles grow a daunting task.

Here we investigate the particle growth behavior of supported nickel catalyst as function of the support type and the size of the Ni nanoparticles in the aqueous phase using the reforming (APR) of

ethylene glycol as a model reaction. These conditions, hot (230 °C) compressed water with a carbohydrate model compound, are relevant to the catalytic processing of biomass feedstock. The supports were selected based on their known stability under these conditions with the addition of γ -Al₂O₃ which was included since it is one of the most used supports in APR. We show that the particle growth observed under these conditions is best described by an Ostwald ripening mechanism with migration of dissolved nickel species through the aqueous phase. Besides the support type, the initial particle sizes as well as the initial particle size distribution are shown to be important parameters that affect the particle growth characteristics.

2. Experimental

The support materials used in this study were α -Al₂O₃ (BASF Al-4196E 1.8 mm), γ -Al₂O₃ (Engelhard, BN 245), ZrO₂ (Degussa, BN132), β -SiC (SiCAT CtS-56) and surface-oxidized carbon nanofibers (CNF, prepared in-house). The catalysts were prepared by incipient wetness impregnation of the support materials with aqueous solutions of Ni(NO₃)₂·6H₂O to obtain a metal loading of approximately 10 wt%. Catalyst characteristics and preparation conditions are shown in Table 1. After impregnation the catalysts were dried in vacuum at room temperature or overnight in air at 80 °C. Next, the catalyst precursor was activated by direct reduction or by calcination in static air or in N₂ flow followed by reduction in 33% H₂ in N₂ (150 mL/min). After the reduction treatment part of the sample was passivated by controlled exposure to air before characterizing with XRD and TEM.

The stability of the supported Ni catalysts was investigated during the aqueous phase reforming of ethylene glycol. Typically 100 mg catalyst (90–220 μ m sieve fraction) was loaded into a 10 mL batch autoclave reactor (Swagelok union mini-reactors similar to those reported in [21,22]) and 4 mL of 1 wt% aqueous ethylene glycol solution was added using a volumetric pipet. The reactor was filled in a glove box under inert atmosphere. The reactant solution was degassed with argon gas prior to its introduction into the glove box in order to prevent oxidation of the freshly reduced catalyst by dissolved oxygen. Next the reactor was placed in a preheated (230 °C) tumbling oven (4 rpm) as previously reported [23].

Fresh and spent catalysts were characterized by X-Ray powder diffraction (XRD), H₂ chemisorption, and Transmission Electron Microscopy (TEM). Powder X-ray diffraction (XRD) was measured using an D2 PHASER X-ray Diffraction Analyzer from Bruker with Co K α radiation (λ = 1.789 Å). Nickel crystallite sizes of the reduced and passivated catalysts were estimated with the Scherrer equation using a shape factor of 0.89. Values for the full width at half maximum for Ni (111) were obtained from a least squares fit of the experimental data with a pseudo-Voigt function by

Table 1. Overview of catalyst preparation conditions and sample treatment history with resulting nickel particle sizes obtained from XRD and H₂-chemisorption.

Sample code	Ni ^a (wt%)	Drying (°C)	Cal ^b (°C)	Red ^c (°C)	BET area ^d (m ² /g)	Ni particle size (nm)		
						d_{XRD}^e	$d_{\text{H}_2\text{C}}^f$	d_{TEM}
Ni/ γ -Al ₂ O ₃	9.2	80	600 (air)	500 (2 h)	185	4	14	~5 to 10
Ni/ZrO ₂	9.5	80	600 (air)	500 (2 h)	81	10	8.7	–
Ni/SiC	9.8	80	600 (air)	500 (2 h)	23	16	–	–
Ni/CNF	9.8	80	–	300 (2 h)	173	6	4	–
20Ni/ α -Al ₂ O ₃	9.8	80	500 (air)	500 (2 h)	7	20	24	22
12Ni/ α -Al ₂ O ₃	9.8	vacuum	400 (N ₂)	400 (1 h)	7	12	9.1	12
2%Ni/ α -Al ₂ O ₃	2.0	vacuum	–	500 (1 h)	7	13	–	–

^a Nominal nickel loading.

^b Calcination (cal) treatment in static air or N₂ flow (150 mL/min) at the designated temperature with a 5 °C/min heating ramp for 2 h.

^c Reduction treatment (red) in 30% H₂ in N₂ (total flow 150 mL/min) at the designated temperature with a 5 °C/min heating ramp.

^d Specific surface area of the support material according to the BET method.

^e Average nickel crystallite sizes as determined by XRD (d_{XRD}).

^f Average nickel particle sizes as determined by hydrogen chemisorption ($d_{\text{H}_2\text{C}}$).

deconvolution of support and metal contributions with a correction for instrumental broadening. Hydrogen chemisorption was performed on a Micromeritics ASAP 2020C instrument. The passivated catalyst was re-reduced in H_2 (60 mL/min) at 300 °C for 2 h. The monolayer H_2 uptake was found by extrapolating the linear part of the isotherm (150–600 mbar) to zero pressure. Particle sizes were calculated using the monolayer uptake assuming complete reduction and a stoichiometry of 1 hydrogen atom per metal surface atom for all samples. The passivated samples were further examined with transmission electron microscopy (TEM) using an FEI Tecnai 12. The samples were placed on holey carbon grid and both bright field and dark field TEM images were recorded.

3. Results and discussion

Fig. 1 shows the XRD patterns for Ni on different supports for both the parent and spent catalysts (after 22 h reaction time). For parent 20Ni/ α - Al_2O_3 and Ni/SiC the contribution of the Ni (53° and 61° of 2 theta) can be clearly distinguished from those of the support materials. For the other catalysts where the Ni and support contributions partially overlap, the Ni contributions were estimated by deconvolution of the support and nickel diffraction lines. The Ni crystallite size obtained for the parent catalysts are given in Table 1 together with those obtained by hydrogen chemisorption. The values are in reasonable agreement for most samples. The larger value of the Ni particle size on γ - Al_2O_3 obtained by H_2 chemisorption compared to XRD and TEM was likely due to incomplete reduction of the NiO and Ni-aluminate. No NiO diffraction lines were observed for any of the samples although a contribution of $NiAl_2O_4$ (72° 2 theta) for the Ni/ γ - Al_2O_3 sample cannot be excluded. For the spent catalyst no observable changes occurred in the XRD patterns to any of the support materials except for γ - Al_2O_3 for which a transformation into a boehmite phase occurred (see Fig. S1 for more details). More narrow diffraction peaks with increased intensity were observed for Ni in all the spent catalyst which shows growth of the Ni crystallites occurred during the APR treatment.

TEM micrographs of parent and spent catalysts (after 22 h) for Ni/ZrO₂ and Ni/ γ - Al_2O_3 are displayed in Fig. 2. For the parent Ni/ZrO₂ (Fig. 2a) we could not observe any nickel particles. Analysis with EDX line-scans (Fig. 2a) showed however that the nickel

is well distributed over the support since the intensity curves of Ni and Zr perfectly match each other. The spent Ni/ZrO₂ sample (Fig. 2b) showed very large Ni particles and areas with large Ni clusters of up to half a micrometer, as was confirmed by EDX (Fig. 2b). For the fresh Ni/ γ - Al_2O_3 catalyst it was difficult to identify discrete nickel particles, although 5–10 nm particles could be observed in the less dense areas of the sample. For the spent Ni/ γ - Al_2O_3 sample the Ni particles increased to >50 nm and these particles were easily distinguished from the support material. In addition a change in shape of the support was observed which was due to the transformation of the γ - Al_2O_3 to boehmite as was already observed with XRD.

For 20Ni/ α - Al_2O_3 catalysts the nickel particles could be readily observed and the influence of particle size on stability was further investigated in more detail (Fig. 3). For the parent 20Ni/ α - Al_2O_3 catalyst (Fig. 3a) particles with an average size of 22 nm were observed which increased to 44 nm for the spent catalyst (Fig. 3b). The particle size distribution (Fig. 3g) showed that most (40%) of the particles were between 10 and 20 nm for the fresh catalysts while in the spent catalysts most of the Ni particles (25%) were 30–40 nm, resulting in a shift and broadening of the size distribution (average size 44 nm). Fig. 3(c) shows micrographs for the fresh 12Ni/ α - Al_2O_3 in both bright field (Fig. 3c) and dark field (Fig. 3d). Clearly this catalyst has smaller nickel particles and thus a higher dispersion than 20Ni/ α - Al_2O_3 catalyst. For 12Ni/ α - Al_2O_3 more than 90% of the particles were below 20 nm (average size of 12 nm). For the spent 12Ni/ α - Al_2O_3 catalyst (Fig. 3e and f) the particles increased in size to 20–40 nm with also a significant amount of very large particles >100 nm (Fig. 3h) resulting a bimodal size distribution (average size of 58 nm).

The growth of Ni particles during the reforming of 1 wt% ethylene glycol was followed over time for 10 wt% Ni catalysts supported on ZrO₂, CNF, SiC, γ - Al_2O_3 and α - Al_2O_3 . The nickel crystallite growth curves as determined by XRD analysis are shown in Fig. 4(a). Notable differences in the extent of growth between the various supports are apparent from Fig. 4(a). For all the investigated supports the most extensive part of the Ni particle growth occurs already in the first four hours of the reaction and the extent of the Ni growth follows the order CNF > ZrO₂ > SiC > γ - Al_2O_3 > α - Al_2O_3 . Interestingly, the 20Ni/ α - Al_2O_3 had the largest initial particle size of all these catalyst and showed not only the

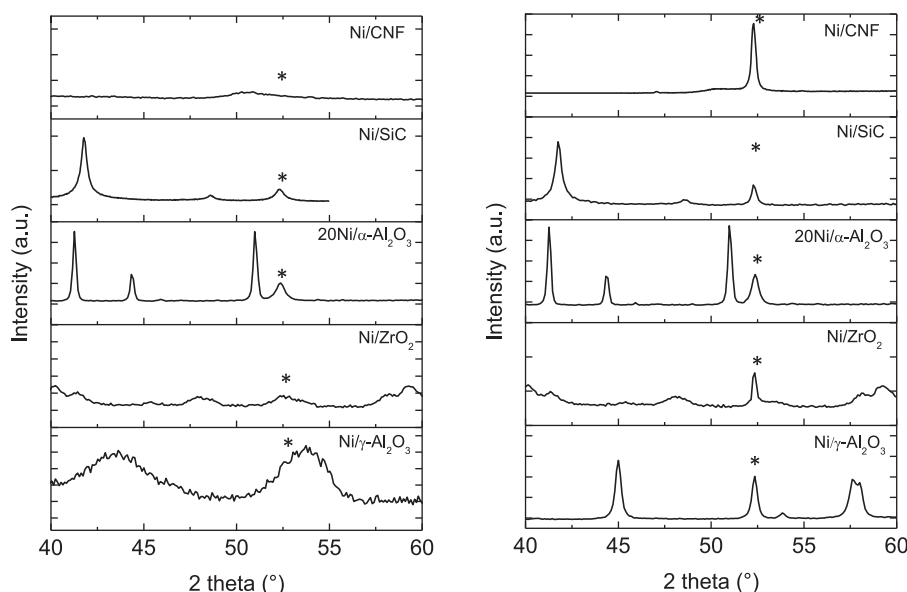


Fig. 1. XRD diffractograms of passivated parent nickel catalyst (left pane) and after 22 h reaction (right pane) showing the Ni (*) contributions.

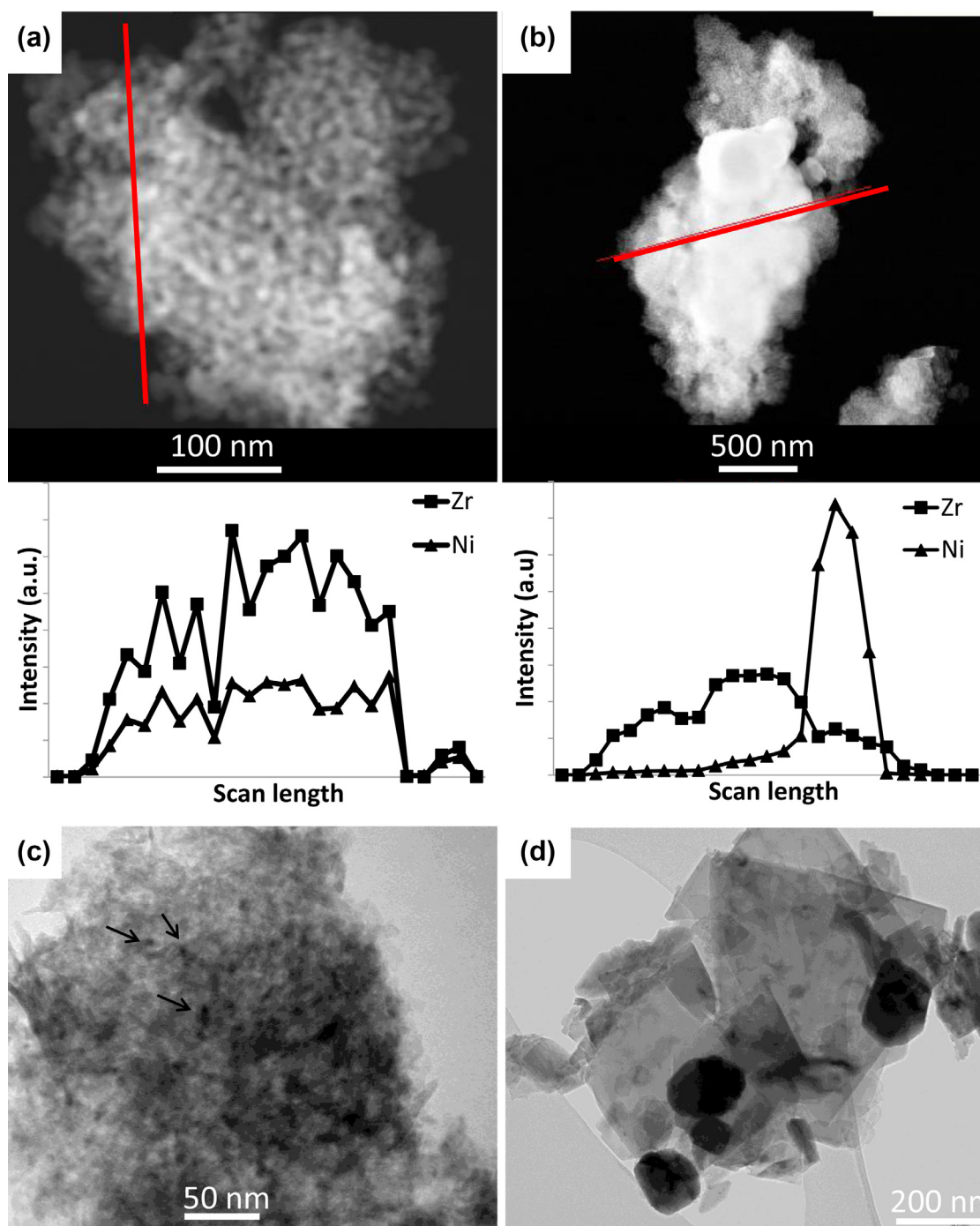


Fig. 2. (a) TEM dark field of parent Ni/ZrO₂ with corresponding EDX line profiles of Ni and Zr below, (b) TEM dark field image of Ni/ZrO₂ spent after 22 h reaction with corresponding EDX line profiles of Ni and Zr below and (c) TEM bright field of the parent Ni/ γ -Al₂O₃ with nickel particles indicated by arrows and (d) TEM bright field of the spent Ni/ γ -Al₂O₃ catalyst after 22 h reaction.

lowest growth rate but also had the smallest Ni particle size at the end of the reaction.

With the variation of the support type concurrent changes were introduced to other parameters, besides changes in the metal support interactions. Two of these parameters, the inter-particle distance (IPD) and the particle size, are likely relevant to the growth behavior of Ni particles. First of all the employed supports have specific surface areas varying more than a factor 30 (between 7 and 185 m²/g, see Table 1) and as such the particle density and thus the inter-particle distance of the Ni particles will vary. Secondly the initial crystallite size of these catalysts (as show in

Table 1) varies about of factor of five, between 4 and 20 nm. In order to study the effect of the initial particle size on the growth characteristics, additional samples of Ni supported on α -Al₂O₃ were investigated with respect to the rate of particle growth. Using different preparation procedures (see Table 1) a sample with approximately 12 nm nickel particles (12Ni/ α -Al₂O₃) was prepared (see Fig. 3e and f), which is significantly smaller than the 20 nm average of the 20Ni/ α -Al₂O₃ sample. An additional sample (2%Ni/ α -Al₂O₃) was prepared with a 5 times lower loading of Ni (i.e. 2 wt%) but with the same particle size as 12Ni/ α -Al₂O₃, i.e. 13 nm (see Table 1). The three different α -Al₂O₃ catalysts thus

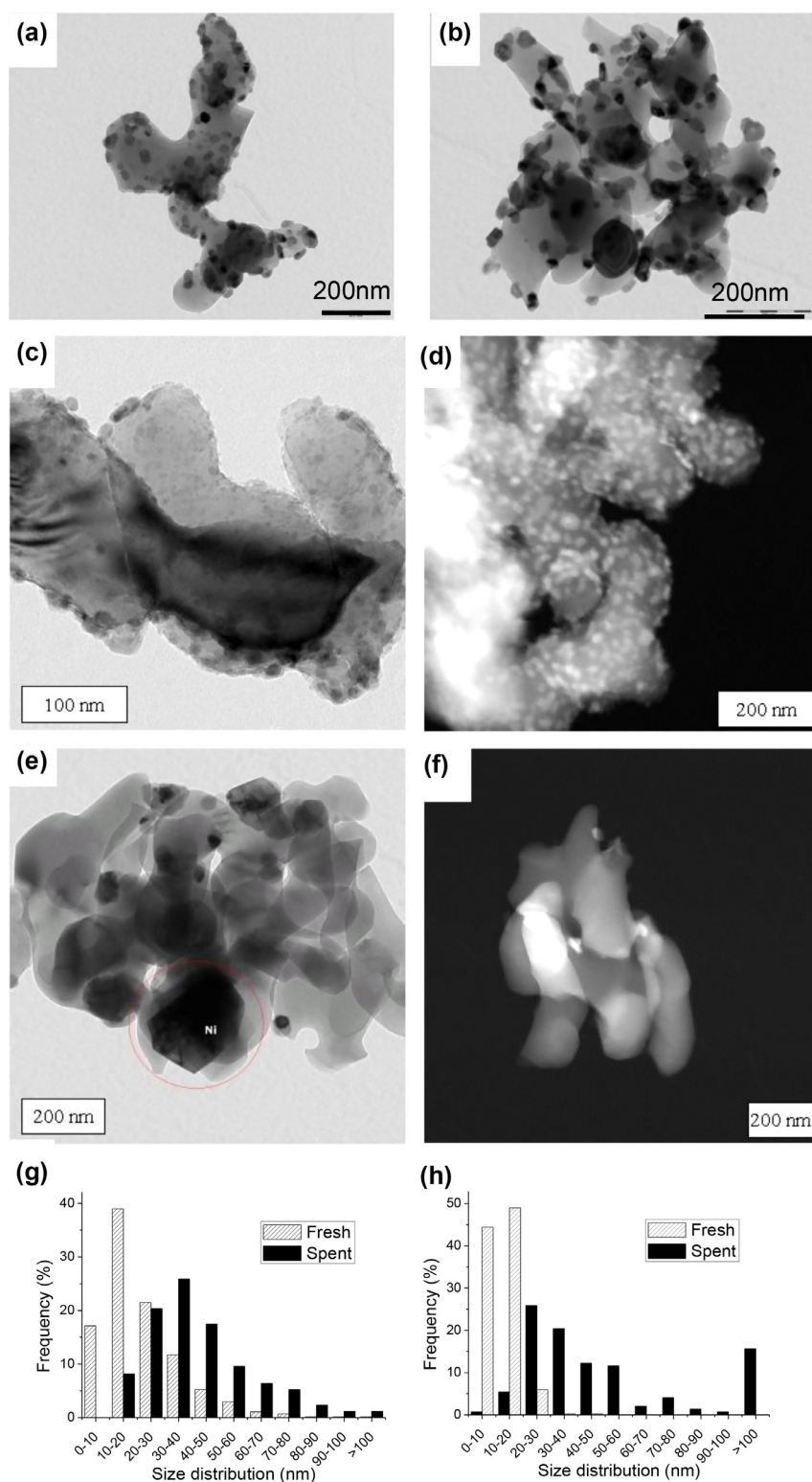


Fig. 3. TEM images of (a) parent 20Ni/α-Al₂O₃, (b) spent 20Ni/α-Al₂O₃ after 22 h reaction, (c) parent 12Ni/α-Al₂O₃ (bright field), (d) parent 12Ni/α-Al₂O₃ (dark field), (e) spent 12Ni/α-Al₂O₃ after 22 h reaction, and (f) spent 12Ni/α-Al₂O₃ after 22 h reaction (dark field). Histograms of parent and spent (after 22 h reaction) catalyst particle size distribution of (g) 20Ni/α-Al₂O₃ and (h) 12Ni/α-Al₂O₃ catalysts.

vary in initial nickel particle size and inter-particle distances. The Ni growth curves of these catalysts are displayed in Fig. 4(b). The differently prepared Ni/α-Al₂O₃ samples also show large variations in the growth characteristics. The fastest particle growth was observed for the 12Ni/α-Al₂O₃ catalyst followed by the 2Ni/α-Al₂O₃ catalyst. Both of these catalysts have a higher particle growth rate than the 20Ni/α-Al₂O₃ catalyst which had a larger initial

particle size. Also, their final particle size far exceeds that of 20Ni/α-Al₂O₃. The 2Ni/α-Al₂O₃ catalyst with the lower nickel loading showed a less extensive growth than the 12Ni/α-Al₂O₃ with comparable initial particle size.

In order to compare the extent of particle growth for the various catalysts with different initial particle size we plotted the particle growth factor (initial particle size divided by the final

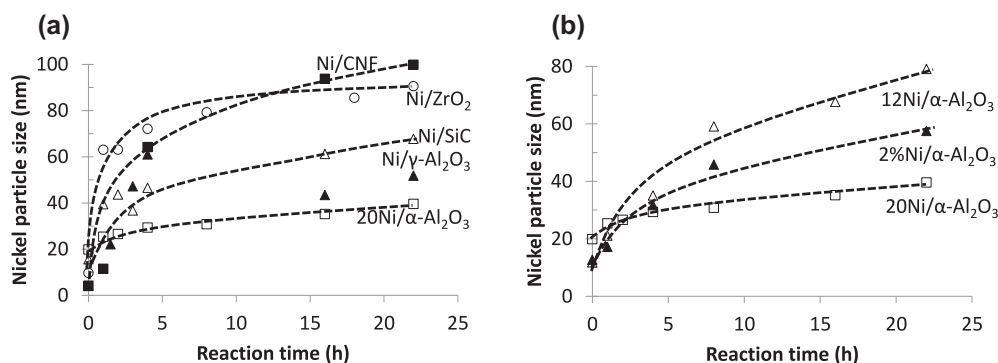


Fig. 4. Nickel particle growth curves of Ni catalyst on various supports (a) and of Ni/α-Al₂O₃ catalyst (b) prepared using the synthesis conditions outlined in Table 1 during the APR of 1 wt% EG at 230 °C.

particle size) versus the calculated inter-particle distance (IPD) and the particle size. A plot of the calculated inter-particle distance (based on the initial particle size and the specific surface area of the support, see supporting information for more details) versus growth factor after 22 h for all catalysts is shown in Fig. 5(a). No relationship between the inter-particle distance and the growth factor for the different catalysts was observed. The effect of the initial particle size on the particle growth factor for the different samples in this study is shown in Fig. 5(b). This figure shows that the initial particle size appears to have an inverse correlation with the initial particle size.

4. Discussion

The particle growth behavior of Ni on various supports and Ni supported on α-Al₂O₃ with different initial particle sizes shows that the support type is not the only important factor in the growth process and the support effect are overshadowed by the large effect of the initial particle size (Fig. 4a and b). Since catalyst with initially smaller particles show more rapid and more extensive growth it appears that the lower growth rate of the 20Ni/α-Al₂O₃ sample compared to the other supports, as shown in Fig. 4(a), is not inherent to the support type but is related to the initial particle size or the particle size distribution. The higher growth rate observed for smaller particles is expected based on known particle growth mechanisms, i.e. Ostwald ripening (OR) and particle migration and coalescence (PMC). If particle growth occurs via particle migration and coalescence (PMC) more rapid growth is expected for smaller particle because they are more mobile. A higher growth rate is also expected for smaller particles if particle growth

occurs via Ostwald ripening because of their higher solubility (due to their excess surface energy).

The type of growth mechanism is of interest since this knowledge can aid in the development of strategies to combat particle growth. Based on the result presented here a definitive conclusion with respect to the growth mechanism cannot be drawn. However, several observations made point towards Ostwald ripening as the growth mechanism. First of all substantial levels of dissolved Ni were detected in the liquid phase with Atomic Absorption Spectroscopy (AAS) for both Ni/ZrO₂ (~60 to 160 ppm) and 20Ni/α-Al₂O₃ (~5 to 30 ppm), see Fig. S2. Whereas for Pt based catalysts particle growth via Ostwald ripening in liquid phase reactions has been dismissed on the grounds that the solubility of Pt in the aqueous phase is too low [14], the much higher solubility of Ni species in the aqueous phase makes mass transport via dissolved species a realistic possibility. Secondly, because the coalescence in PMC is much faster than the transport of the particle over the support surface, the latter is the rate determining step [19] and the growth rate is proportional to the particle distance or density. Such a relation was not observed in Fig. 5(a). Furthermore, a strong argument for the prevalence of Ostwald ripening as the growth mechanism is the absence of the influence of the catalyst loading on the growth rate [24]. In the PMC mechanism the rate constant is directly proportional to the metal loading (and IPD) for a comparable particle sizes. It is difficult to determine the rate constant from Fig. 4(b) because the initial particle growth rates are very high. However, the initial particle growth rate of the sample with the lower loading (2%Ni/α-Al₂O₃) does not appear to differ substantially from that of 12Ni/α-Al₂O₃ which has a 5 times higher loading and a comparable initial particle size. Another observation

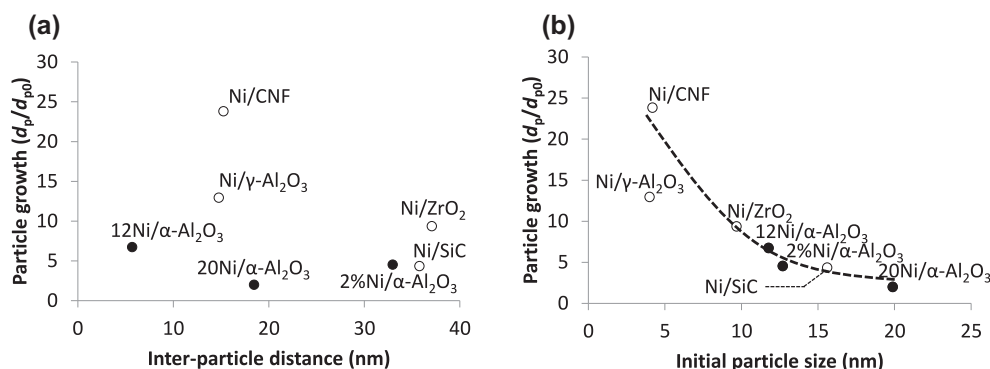


Fig. 5. Effects of the theoretical inter-particle distance (IPD) (a) and the initial particle size (b) on the growth factor (d_p/d_{p0}) for Ni supported on γ-Al₂O₃, CNF, SiC ZrO₂ (open symbols) and α-Al₂O₃ (closed symbols) after treatment for 22 h in a 1 wt% ethylene glycol solution at 230 °C.

that points towards Ostwald ripening as the growth mechanism is that, even after extensive particle growth (when mainly very large particle are present) still some very small particles can be observed (see for instance Fig. 3e). This can best be explained by the Ostwald ripening mechanism because during large and small particles are expected to be present simultaneously because the larger particles grow at the expense of shrinking smaller particles. Lastly, it was observed that in some cases the Ni particle growth is so extensive that they grow as large as the support particle/crystallites themselves (Figs. 2b and 3e). This observation was used as argument by Flynn et al. [20] in favor of the OR growth mechanism since it shows that transport of Ni must take place over the boundaries of the support particles/crystallites, making migration of whole nickel particles unlikely.

Finally, the observation that the nickel particles of 12Ni/ α -Al₂O₃ with the initially smaller particles “outgrow” those of the sample with the initially larger particles (20Ni/ α -Al₂O₃) is also remarkable, i.e. the smaller particles 12 nm have a higher initial growth rate than the larger 20 nm particles but the growth rates do not equilibrate as the size difference becomes smaller. This behavior is in direct contradiction with both generalized Ostwald ripening theory by Lifshitz–Slyozov–Wagner [19] and theories on particle migration because, although these theories predict that the initial rate of particle growth is larger for smaller particle, the rate will also decrease as the average particle size increases. However, Munnik et al. [25] recently found that during Ostwald ripening of nickel particles in gas phase methanation experiments the small Ni particles deactivated faster due to particle growth and to a larger extent than catalysts with medium sized particles. Also, Ferreira et al. [26] found that Pt/C membrane cathode catalysts with the smallest particles actually end up with the largest particles after potential cycling. This is in line with Fig. 4(b), which shows that during the growth process the particle size of the 12Ni/ α -Al₂O₃ catalyst with the smallest initial size (12 nm) exceeded the size for the sample (20Ni/ α -Al₂O₃) with an initially larger average Ni size (20 nm). This phenomenon could be the result of the difference in initial particle size and particle size distribution due to the fact that small Ni particles are more easily oxidized, which is a requirement for the particle growth via OR. Because the smaller nickel particle are more susceptible to oxidation and leaching they are the main source of leached species while the re-deposition and re-reduction of leached nickel is favored on the larger particles with a more metallic surface that can dissociate the hydrogen needed for the reduction of metal ions. For different size distributions the growth rate can also differ even if the average particles size is the same [27]. For the 12Ni/ α -Al₂O₃ sample the initial average particle size (12 nm) was close to what is practically attainable while the distribution appears to be relatively narrow. However for this sample (12Ni/ α -Al₂O₃) some larger particles were observed which did not have a significant contribution to the histogram in Fig. 3, e.g. less and 0.6% of the particles have a size larger than 50 nm). The small particles in the vicinity of the scarce number of very large particles will result in a much larger concentration gradient between dissolved nickel species compared to the distribution of 20Ni/ α -Al₂O₃. As a result the Ni flux between these particles is larger which means a much larger growth rate of the anomalous large particles in this sample. Using a theoretical model it has been shown that the introduction of a large particle in a distribution of small particles can already significantly affect the growth behavior of the population [27] which was confirmed experimentally by van den Berg et al. [28] for Cu supported on silica during methanol synthesis. It has also been shown previously that the local distribution can have a significant impact on the overall metal particle growth behavior of a catalyst [7].

5. Conclusions

The effect of support type and particle size on Ni particle growth was investigated for Ni nanoparticles supported on CNF, ZrO₂, SiC, γ -Al₂O₃ and α -Al₂O₃. The extent of the Ni growth varied among the different support materials, however the Ni particle growth was found to be related to the initial nickel particle size which overshadowed the effect of the support material. Nickel supported on α -Al₂O₃ with different initial particle sizes and loadings also showed that the initial particle size is the most important parameter determining the rate of particle growth. A Ni/ α -Al₂O₃ catalyst with an initial particle size of 12 nm showed faster and more extensive growth than a Ni/ α -Al₂O₃ catalyst with an initial particle size of 20 nm. Furthermore, the sample with the initially smaller particles was found to outgrow the catalyst with the larger particles. Ostwald ripening is thought to be the most likely particle growth mechanism and it is postulated that the unusual growth behaviors could be related to the increased susceptibility of smaller nickel particle with respect to oxidation. Also the presence of some larger particles in the catalyst with an average particle size of 12 nm probably enhanced the concentration gradient between the particles and increased the particle growth rate compared to the catalyst with an initial particle size of 20 nm.

Acknowledgments

The authors gratefully acknowledge Cor van der Speck for TEM analysis.

Supplementary materials

Supplementary material associated with this article can be found, in the online version, at doi:10.1016/j.jechem.2016.01.006.

References

- [1] T. van Haasterecht, C.C.I. Ludding, K.P. de Jong, J.H. Bitter, *J. Energy Chem.* 22 (2013) 12.
- [2] T. van Haasterecht, C.C.I. Ludding, K.P. de Jong, J.H. Bitter, *J. Catal.* 319 (2014) 27–35.
- [3] T. van Haasterecht, T.W. van Deelen, K.P. de Jong, J.H. Bitter, *Catal. Sci. Technol.* 4 (2014) 2353–2366.
- [4] G.W. Huber, J.W. Shabaker, J.A. Dumesic, *Science* 300 (2003) 2075–2077.
- [5] J. Sehested, J.A.P. Gelten, I.N. Remediakis, H. Bengaard, J.K. Nørskov, *J. Catal.* 223 (2004) 432–443.
- [6] G. Prieto, J.D. Meeldijk, K.P. de Jong, P.E. de Jongh, *J. Catal.* 303 (2013) 31–40.
- [7] G. Prieto, J. Zecevic, H. Friedrich, K.P. de Jong, P.E. de Jongh, *Nat. Mater.* 12 (2013) 34–39.
- [8] F. Beharfarid, B. Roldan Cuenya, *Top. Catal.* 56 (2013) 1542–1559.
- [9] C.H. Bartholomew, *Studies in Surface Science and Catalysis*, Elsevier, 1994, pp. 1–18.
- [10] C. Montassier, J.M. Dumas, P. Granger, J. Barbier, *Appl. Catal. A: Gen.* 121 (1995) 231–244.
- [11] J.W. Shabaker, D.A. Simonetti, R.D. Cortright, J.A. Dumesic, *J. Catal.* 231 (2005) 67–76.
- [12] J.F. Connolly, R.J. Flannery, B.L. Meyers, *J. Electrochem. Soc.* 114 (1967) 241–243.
- [13] J.A.S. Bett, K. Kinoshita, P. Stonehart, *J. Catal.* 41 (1976) 124–133.
- [14] J.H. Vleeming, B.F.M. Kuster, G.B. Marin, F. Oudet, P. Courtine, *J. Catal.* 166 (1997) 148–159.
- [15] A. Doudah, P. Marécot, S. Labruquère, J. Barbier, *Appl. Catal. A: Gen.* 210 (2001) 111–120.
- [16] A. Doudah, P. Marécot, J. Barbier, *Appl. Catal. A: Gen.* 225 (2002) 11–19.
- [17] A. Doudah, P. Marécot, S. Szabo, J. Barbier, *Appl. Catal. A: Gen.* 225 (2002) 21–31.
- [18] Y. Shao-Horn, W.C. Sheng, S. Chen, P.J. Ferreira, E.F. Holby, D. Morgan, *Top. Catal.* 46 (2007) 285–305.
- [19] P. Wynblatt, N.A. Gjostein, *Prog. Solid State Chem.* 9 (1975) 21–58.
- [20] P.C. Flynn, S.E. Wanke, *J. Catal.* 34 (1974) 390–399.
- [21] T.D. Matson, K. Barta, A.V. Iretskii, P.C. Ford, *J. Am. Chem. Soc.* 133 (2011) 14090–14097.
- [22] K. Barta, T.D. Matson, M.L. Fetting, S.L. Scott, A.V. Iretskii, P.C. Ford, *Green Chem.* 12 (2010) 1640–1647.

- [23] S.C.C. Wiedemann, J.A. Stewart, F. Soulimani, T. van Bergen-Brenkman, S. Langelaar, B. Wels, P. de Peinder, P.C.A. Bruijnincx, B.M. Weckhuysen, *J. Catal.* 316 (2014) 24–35.
- [24] W.J. Dunning, *Particle Growth in Suspensions*, Academic Press, 1973.
- [25] P. Munnik, M.E.Z. Velthoen, P.E. de Jongh, K.P. de Jong, C.J. Gommès, *Angew. Chem. Int. Ed.* 53 (2014) 9493–9497.
- [26] K. Yu, D.J. Groom, X. Wang, Z. Yang, M. Gummalla, S.C. Ball, D.J. Myers, P.J. Ferreira, *Chem. Mater.* 26 (2014) 5540–5548.
- [27] P.C. Flynn, S.E. Wanke, *J. Catal.* 34 (1974) 400–410.
- [28] R. van den Berg, T.E. Parmentier, C.F. Elkjær, C.J. Gommès, J. Sehested, S. Helveg, P.E. de Jongh, K.P. de Jong, *ACS Catal.* 5 (2015) 4439–4448.